Nanoscale

This is an *Accepted Manuscript*, which has been through the Royal Society of Chemistry peer review process and has been accepted for publication.

Accepted Manuscripts are published online shortly after acceptance, before technical editing, formatting and proof reading. Using this free service, authors can make their results available to the community, in citable form, before we publish the edited article. We will replace this *Accepted Manuscript* with the edited and formatted *Advance Article* as soon as it is available.

You can find more information about *Accepted Manuscripts* in the **Information for Authors**.

Please note that technical editing may introduce minor changes to the text and/or graphics, which may alter content. The journal's standard **Terms & Conditions** and the **Ethical guidelines** still apply. In no event shall the Royal Society of Chemistry be held responsible for any errors or omissions in this *Accepted Manuscript* or any consequences arising from the use of any information it contains.

Biodegradable nanoassemblies of piperlongumine display enhanced antiangiogenesis and antitumor activities

Yuanyuan Liu [a,1], Ying Chang [a,1], Chao Yang [a,1], Zitai Sang [a], Tao Yang [a], Wei Ang [b], Weiwei Ye [a], Yuquan Wei [a], Changyang Gong [a,*], Youfu Luo [a,*]

[a] State Key Laboratory of Biotherapy, West China Hospital, West China Medical School, Sichuan University, Chengdu, Sichuan 610041, PR China
[b] Key Laboratory of Drug Targeting and Drug Delivery System, Ministry of Education, West China Medical School, Sichuan University, Chengdu, Sichuan 610041, PR China

* Corresponding author: State Key Laboratory of Biotherapy, West China Hospital, West China Medical School, Sichuan University, Chengdu, Sichuan 610041, PR China. Tel/fax: +86 28 85503817 (Y Luo). E-mail address: luo_youfu@scu.edu.cn (Y Luo) and chygong14@163.com (C Gong).

[1] These authors contributed equally to this work.

Abstract

Piperlongumine (PL) showed an inhibitory effect on tumor growth; however, lipophilicity restricted its further applications. Nanotechnology provides an effective method to overcome the poor water solubility of lipophilic drugs. Polymeric micelles with small particle size can passively target to tumors by the enhanced permeability and retention (EPR) effect, thus improving their anti-tumor effects. In this study, to improve water solubility and anti-tumor activity of PL, PL encapsulated polymeric micelles (PL micelles) were prepared by a solid dispersion method. The prepared PL micelles showed small particle size and high encapsulation efficiency, which could be lyophilized into powder and the re-dissolved PL micelles are homogenous and stable in water. In addition, a sustained release behavior of PL micelles was observed *in vitro*. Encapsulation of PL into polymeric micelles could increase the cytotoxicity, cellular uptake, reactive oxygen species (ROS) and oxidized glutathione (GSSG), and reduce glutathione (GSH) levels *in vitro*. Besides, encapsulation of PL into polymeric micelles enhanced its inhibitory effect on neovascularization both *in vitro* and *in vivo*. Compared with free PL, PL micelles showed a stronger inhibitory effect on the proliferation, migration, invasion and tube formation of human umbilical vein endothelial cells (HUVECs). Besides, in a transgenic zebrafish model, embryonic angiogenesis was inhibited by PL micelles. Furthermore, PL micelles were more effective in inhibiting tumor growth and prolonging survival in subcutaneous CT-26 murine tumor model *in vivo*. Therefore, our data revealed that the encapsulation of PL into biodegradable polymeric micelles enhanced its anti-angiogenesis and anti-tumor activities both *in vitro* and *in vivo*.

1. Introduction

Cancer is one of the most severe human diseases in the world, with an increasing morbidity and mortality. Enhanced cellular stress (for example, oxidative, loss of glutathione (GSH)/oxidized glutathione (GSSG) balance) is frequently associated with cell deregulation, which is important for cancer cell apoptosis.[1] Small molecules, which alter levels of reactive oxygen species (ROS) and cause oxidative stress for tumor cells, have been suggested as a treatment of cancer.[2, 3] Besides, tumor progression is highly dependent on angiogenesis, and angiogenesis assists tumor cells to leave the primary site and enter circulation, facilitating tumor metastasis.[4, 5] Combinational strategy of anti-angiogenesis and selective killing tumor cells by targeting certain specified biological targets or increasing cellular ROS level is an important direction of tumor therapy.

Medicine derived from plants play a highly significant role in the healthcare of human, both ancient and modern.[6-8] Piperlongumine (PL), an alkaloid/amide component isolated from the plant species *Piper longum Linn*, showed multiple pharmacological activities such as anti-platelet aggregation, antibacterial, insecticidal property, cytotoxic, anti-tumor and anti-angiogenesis.[9-14] Among the multivalent effects, the potential of PL as novel anti-tumor agent has gained increasing attention recently. Previous studies revealed that PL exhibited selective cytotoxicity to tumor cells and show therapeutic effect in suppressing tumor growth in mice.[15] The induction of ROS by inhibiting the ubiquitin–proteasome system (UPS) at a pre-proteasomal step and the proteasome-mediated ROS-dependent mechanism have been reported to contribute to the anti-tumor activity of PL.[13, 16] In addition, protein glutathionylation, glutathione depletion and antiangiogenesis also play important roles in the anti-tumor effects of PL.[1, 17] Besides, PL was proved to be a safe agent for *in vitro* and *in vivo* application, since it has little effect on either slowly or rapidly dividing primary normal cells and no apparent toxicity were found in PL-treated normal mice.[1] However, PL is water-insoluble, of low bioavailability and limited efficacy *in vivo,* which makes it desirable to develop novel drug delivery system for PL to enhance its *in vivo* efficacy.

Nanotechnology provides a novel method to prepare water-based formulation of hydrophobic drugs and attracts increasing attention in drug delivery and cancer therapy.[18-21] Biodegradable polymeric micelles with their core-shell geometry are widely applied as drug delivery system (DDS).[22, 23] Encapsulation of hydrophobic compounds into polymeric micelles renders the drug completely dispersible in water and forms a stable and homogenous solution for intravenous applications.[24-26] Biodegradable polymeric micelles with their ability of prolonging drug circulation time *in vivo* are viewed as excellent candidates for anticancer DDS.[27-29] Furthermore, polymeric nanoparticles with their enhanced permeability and retention (EPR) effect can passively target to tumor tissues, improving their anti-tumor effects.[30-32]

In this work, we prepared PL loaded polymeric micelles (PL micelles), and the anti-angiogenesis and anti-tumor activity of PL micelles were investigated both *in vitro* and *in vivo*. Cytotoxicity, apoptosis, cellular uptake, drug release behavior and anti-angiogenesis activity of PL micelles *in vitro* were studied in detail. We also evaluated the inhibitory effects of PL micelles on embryonic angiogenesis using transgenic zebrafish model. Meanwhile, subcutaneous CT-26 murine tumor model was established to investigate the anti-tumor activity of PL micelles *in vivo*. The results suggested that PL micelles improved cellular drug delivery and showed promoted anti-angiogenesis and anti-tumor activity compared with free PL both *in vitro* and *in vivo*, and may have potential applications in anti-tumor therapy.

2. Materials and methods

2.1. Materials, cell lines and animals

Poly(ethylene glycol) methyl ether (MPEG, Mn=2000, Fluka, USA), ε-caprolactone (ε-CL, Alfa Aesar, USA), stannous octoate (Sn(Oct)$_2$, Sigma, USA), piperlongumine (PL, Sigma, USA), methanol (HPLC grade, Fisher Scientific, UK), methyl thiazolyl tetrazolium (MTT, Sigma, USA), Roswell Park Memorial Institute 1640 medium (RPMI 1640, Gibco, USA), fetal bovine serum (FBS, Gibco, USA), Matrigel (BD Biosciences, USA), alginate sodium (Sigma, USA), fluorescein isothiocyanate-dextran (FITC-dextran, Sigma, USA), AnnexinV-FITC/PI Detection kit (keyGEN Biotech, China), GSH/GSSG detection kit (BioAssay, USA), 2',

7'-dichlorofluorescein diacetate (DCF-DA, Sigma, USA) and 1-phenyl-2-thiourea (PTU, Sigma, USA) were used without further purification. All materials used in this study were analytical reagent (AR) grade.

CT-26 cells were purchased from the American Type Culture Collection (ATCC; Rockville, MD). CT-26 cells grew in RPMI 1640 supplement with 10% FBS. Primary human umbilical vein endothelial cells (HUVECs) were obtained from fresh human umbilical cord veins by a standard procedure, and grew in an EBM-2 medium with Single Quots (Lonza) containing VEGF and other growth factors.[33] HUVECs at passages 3 to 6 were used for all experiments. All above cells were incubated at 37 °C under 5% CO_2.

BALB/c mice (18-20 g) were used for *in vivo* anti-tumor tests. Animals were purchased from the Laboratory Animal Center of Sichuan University, which were housed at controlled temperature of 20-22 °C with relative humidity of 50-60% and 12 h light and dark cycles. Mice were provided with standard laboratory chow and tap water *ad libitum*. All mice would be in quarantine for a week before experiment. All procedures were performed following the guideline of the Institutional Animal Care and Treatment Committee of Sichuan University (Chengdu, P.R. China). All mice in this study were treated humanely throughout the experimental period.

2.2. Synthesis and characterization of the copolymer

Using Sn(Oct)$_2$ as the catalyst, MPEG-PCL copolymer was synthesized by a ring-opening polymerization of ε-CL initiated by MPEG, which was reported in previous studies.[23, 34] In brief, MPEG and ε-CL were introduced into a dry glass ampoule with the calculated ratio under a nitrogen atmosphere and a certain amount of Sn(Oct)$_2$ was then added into the reaction vessel under mild agitation, and the reaction system was kept at 130 °C for 6 h. The prepared MPEG-PCL copolymer was characterized using ^1H nuclear magnetic resonance spectroscopy (^1H-NMR, Varian 400 spectrometer, USA), gel permeation chromatography (GPC, Agilent 110 HPLC, USA), and Fourier transform infrared spectroscopy (FTIR, NICOLET 200SXV, USA). At last, the purified MPEG-PCL copolymer was kept in desiccators before use.

2.3. Preparation and characterization of PL micelles

PL micelles were prepared by a one-step solid dispersion method. Briefly, 100 mg of PL and MPEG-PCL copolymer with a ratio (1/19) were dissolved in 5 mL of dehydrated alcohol under mild stirring. Subsequently, the solution was evaporated using a rotary evaporator at 60 °C. During this process, the co-evaporation of PL and MPEG-PCL copolymer was obtained, and PL was distributed in MPEG-PCL copolymer homogenously as an amorphous substance. Then, the co-evaporation was dissolved in normal saline (NS) at 60 °C to self-assemble into micelles with PL encapsulated in. PL micelles were filtered using a 0.22 μm syringe filter (Millex-LG, Millipore, USA), and then were lyophilized and stored at 4 °C before use.

Concentrations of PL were determined by a high performance liquid chromatography (HPLC) instrument and samples were diluted before measurement. The solvent delivery system was equipped with a plus autosampler and a column oven. Detections were taken on a diode array detector (SPD-M20A). Chromatographic separations were performed on a C_{18} column (4.6 mm × 150 mm, 5 μm, Sepax Tec, USA) and the column temperature was kept at 25 °C. Methanol/water (40/60, v/v) was used as the eluent at a flow rate of 1 mL min^{-1}. The detection wavelength was 327.5 nm.

Drug loading (DL) and encapsulation efficiency (EE) of PL micelles were also determined using HPLC. Briefly, 10 mg of lyophilized PL micelles were dissolved in 100 μL of methanol. The amount of PL in the solution was determined by HPLC. The DL and EE of PL micelles were calculated according to equation (1) and (2):

DL= (Amount of PL in polymeric micelles/Amount of PL micelles) × 100% (1)

EE = Experimental drug loading/Theoretical drug loading × 100%   (2)

Particle size distribution and zeta potential of PL micelles were determined using Malvern Nano-ZS 90 laser particle size analyzer at 25 °C. All data were the mean of three test runs, and all results were expressed as mean ± standard deviation (SD). The morphological characteristics of the PL micelles were examined using a transmission electron microscopy (TEM, H6009IV, Hitachi, Japan). PL micelles were diluted with distilled water and then placed on a copper grid covered with nitrocellulose. At last, samples were negatively stained with phosphotungstic acid and dried at room

temperature.

2.4. Cytotoxicity of PL micelles and MPEG-PCL copolymer

Cytotoxicity tests of PL micelles and free PL were performed on CT-26 cells. CT-26 cells were plated at a density of 5×10^3 cells per well in 100 μL of RPMI 1640 in 96-well plates and grown for 24 h. Cells were then exposed to a series of PL micelles at different concentrations for 24 h. Then, the viability of cells was measured by the MTT method. Briefly, the mean percentage of cell survival relative to that of untreated wells was estimated from the data of three individual experiments, and all data were showed as the mean ± SD. In addition, the cytotoxicity evaluation of the MPEG-PCL copolymer was conducted on CT-26 cells using the MTT method presented above.

2.5. Induction of apoptosis by PL micelles

Twenty-four hours after free PL (5 μM) or PL micelle (5 μM) treatment, CT-26 cells were washed with ice-cold phosphate-buffered saline (PBS), subsequently, 5×10^5 of CT-26 cells were stained with Annexin V-FITC for 15 min in the dark followed by AnnexinV-FITC/PI staining. Stained cells were measured by flow cytometry (FCM, BD, USA) and results were expressed as the percentage of early apoptotic cells (AnnexinV$^+$, PI$^-$) and late apoptotic/dead cells (Annexin V$^+$, PI$^+$). The percent of apoptotic cells was normalized to 5% in control medium with 0.1% DMSO. All experiments were made in duplicate and averaged.

2.6. Cellular uptake of PL micelles

For the quantification of the *in vitro* cellular uptake of the PL micelles by CT-26 cells, cells were seeded on 6-well plates with a density of 2×10^5 cells per well and cultured in 2 mL of growth medium. After being incubated for 24 h, growth media were removed and cells were exposed to 2 mL serum-free medium containing blank micelles, free PL, or PL micelles at a final concentration of 5 μmol/mL, respectively. After incubation for 4 or 24 h, the cells were lysed and PL was extracted using methanol and measured by HPLC (Waters Alliance 2695).

2.7. In vitro drug release study

A modified dialysis method was employed to investigate the release behavior of

PL from free PL and PL micelles *in vitro*. Briefly, 1 mL of free PL or PL micelles at a final PL concentration of 1 mg/mL were introduced into dialysis bags (the dialysis area is 1 cm^2 and the molecular mass cutoff is 3.0 kDa). Subsequently, the dialysis bags were incubated in 10 mL of PBS (pre-warmed to 37 °C, pH 7.4) containing Tween80 (0.5% wt). Tubes were placed on a stirrer with a stirring speed of 100 rpm at 37 °C. At specific intervals, all release media were removed and replaced by an equivalent volume of pre-warmed fresh release media. After 10 min of centrifugation, supernatants of the removed release media were collected and stored at 20 °C before analysis. The released PL samples were quantified by HPLC. All results were the mean of five test runs, and all data were expressed as the mean ± SD.

2.8. Assaying of GSH and GSSG

CT-26 cells were treated with PL and PL micelle at a final PL concentration of 5 μM for 3 h. A total number of 1×10^6 cells were collected and centrifuged at 2000 rpm for 5 min and the cell pellets were lysed using ultrasonic irradiation in 100 μL of ice-cold lysis buffer. After being incubated on ice for 10 min, the lysate was centrifuged at 10000 rpm for 10 min and the supernatant was used for GSH and GSSG assay following the manufactures instruction of GSH/GSSG detection kit (BioAssay, USA).

2.9. Detection of ROS

Cells were treated with free PL or PL micelle at a final PL concentration of 5 μM for 24 h. CT-26 cells were rinsed once and then incubated for 20 min at 37 °C with 10 μM 2', 7'-dichlorofluorescein diacetate (DCF-DA; Sigma, USA), a redox-sensitive fluorescent probe, which is cleaved by nonspecific esterase into highly fluorescent DCF. ROS-induced fluorescence intensity of intracellular DCF was measured by flow cytometer (FCM, BD, USA).

2.10. Proliferation, wound healing, transwell invasion, and tube formation assay of HUVECs

Cell proliferation evaluation of HUVECs was measured using MTT as previously described.[35] HUVECs were exposed to a series of free PL, PL micelles for 48 h, respectively. Each assay was replicated 3 times. Then, the mean percentage of

cell survival was calculated.

Wound healing assay was performed using monolayer HUVECs. Briefly, monolayer HUVECs were wounded by scratching with pipette tips and washed with pre-warmed PBS. Subsequently, fresh EBM-2 medium containing blank micelles, free PL (5 μM), or PL micelles at a final PL concentration of 5 μM was added to the scratched monolayers, and EBM-2 medium served as control. After 24 h, images were taken by an OLYMPUS digital camera attached to an inverted microscope. The migrated cells in this assay were quantified by manual counting, and the percentage of inhibition was expressed on the basis of EBM-2 medium-treated cells as 100%.

Invasion assay was performed as described previously with some modifications.[36] The filter of the transwell plate (8.0 μm, Millipore, USA) was coated with 50 μL Matrigel (BD Bioscience). After Matrigel polymerization, the top chambers were seeded with 100 μL EBM-2 medium (without growth factors) containing 2×10^4 of HUVECs, and the bottom chambers of the plate were filled with EBM-2 medium containing various growth factors. Blank micelles, free PL (5 μM), or PL micelles at a final PL concentration of 5 μM was added to top chambers respectively. Cells were allowed to migrate for 24 h. Non-migrated cells were scraped by a cotton swab, and migrated cells were fixed with methanol and stained with 0.05% crystal violet. Migrated cells were photographed under a light microscope and quantified by manual counting. The percentage of migrated cells inhibited by PL micelles was calculated using EBM-2 medium treated wells as 100%.

The tube formation assay was done as described previously.[37] 24-well culture plates coated with 300 μL Matrigel per well were allowed to polymerize at 37 °C for 30 min. Subsequently, HUVECs suspended in EBM-2 medium were seeded onto the Matrigel. Then, and the cells were treated with blank micelles, free PL, or PL micelles, respectively. After 6 h, cells were photographed by a digital camera attached to an inverted microscope.

2.11. Anti-angiogenesis in transgenic zebrafish model

FLK-1 promoter EGFP transgenic (FLK-1: EGFP) zebrafish line (provided by Shuo Lin, UCLA, Los Angeles, CA) was used in our studies. The bright and

consistent green fluorescence of blood vessels in transgenic zebrafish embryos enable investigating anti-angiogenesis activity of drugs.

Twenty embryos per group were used in our experiment, and each experiment was carried out in three independent replicates. All embryos were maintained in Holtfreter's solution (containing PTU) at 28 °C in a humidified incubator.[38] Fifteen hours post fertilization (hpf), embryos were treated with blank micelles, free PL (5 μM), or PL micelles (5 μM) overnight, respectively. At 30 hpf, embryos were stripped off the egg sheath and anesthetized with 0.01% tricaine. Then, images were taken under a confocal microscope (DM6000 CS, Leica, Germany)

2.12. Alginate-encapsulated tumor cell assay

An alginate-encapsulated tumor cell assay was conducted as described.[39] Briefly, alginate beads containing 5×10^4 CT-26 cells per bead were formed and subcutaneously implanted into both dorsal sides of mice. Then mice were injected intravenously every other day with NS (control), blank micelles, free PL (5 mg/kg), or PL micelles (5 mg/kg) for 12 days. At the end of experiment, 100 μL of 0.2% FITC-dextran was injected into mice intravenously. Alginate beads were photographed and removed within 20 min after being exposed surgically. Then each bead was cut up in 1 mL NS and centrifuged to determine the uptake of FITC-dextran by measuring the fluorescence.

2.13. In vivo tumor models and treatment plan

CT-26 tumors were established by subcutaneously injection of 5×10^5 cells in the right flank at day 0. After 6 days, mice bearing tumors around 100 mm^3 were selected and randomized into four groups (12 mice per group). The dosing schedules were NS (control), blank micelles, free PL (5 mg/kg) or PL micelles (5 mg/kg) every other day intravenously. For the tumor growth inhibition study (6 mice per group), tumor length and width were determined every three days using callipers. Tumor volume was calculated by the following formula: tumor volume = $0.52 \times$ length $\times$ width^2. At the end of the experiment, mice were sacrificed. Solid tumors were harvested and processed for immunohistochemical analysis and terminal deoxynuleotidyl transferase–mediated dUTP nick-end labeling (TUNEL) assay. To

further investigate the anti-tumor activity of PL micelles in subcutaneous murine CT-26 colon tumor model, survival times of the mice were recorded (6 mice per group). Besides, for the study of toxicity, the body weight and conditions of mice were monitored every two days.

2.14. Detection of microvessel density (MVD)

The anti-angiogenesis activity of PL micelles was determined by immunohistochemistry analysis of vessel density in tumor tissue.[40] Briefly, frozen sections of CT-26 tumors were fixed in acetone, washed with PBS and then stained with an anti-CD31 antibody (1:50; Abcam, USA). The numbers of microvessels per high-power field in sections were counted using a microscope in each group.

2.15. Assessment of apoptosis

Cell apoptosis in CT-26 tumors was determined by a TUNEL assay. Briefly, tumors tissues in subcutaneous CT-26 model were harvested, fixed in 4% wt paraformaldehyde, embedded in paraffin, and sectioned. Three tumors per group were randomly chosen and analyzed. The TUNEL assay was carried out following the manufacturer's instructions (Promega, USA). The number of TUNEL-positive cells was quantified using fluorescence microscopy, and the apoptotic indexes in 5 randomly selected areas were calculated in each tumor sample in a blinded fashion. The apoptotic index was determined as a ratio of the apoptotic cell number to the total cell number in each high-power field.

2.16. Immunohistochemical determination of Ki-67

Sections of tumor tissue were prepared as described above for Ki-67 staining by the labeled streptavidin-biotin method.[41] The primary antibody and secondary antibody were rabbit anti-mouse monoclonal anti-Ki-67 antibody (Cell Signaling Test, USA) and biotinylated goat anti-rabbit immunoglobulin (BD Biosciences Pharmingen), respectively. The Ki-67 labeling index (Ki-67 LI) was calculated to quantify Ki-67-positive cells/total number of cells. The number of Ki-67-labled cells was quantified under $\times 400$ magnification, and the labeling index in 5 random fields per group was counted in a blinded fashion by two independent investigators.

2.17. Statistical analysis

Statistical analysis was performed by Student's t-test and one-way analysis of variance (ANOVA) using SPSS 11.5 software. Data were expressed as the mean value ± SD. Differences were considered significant if $p < 0.05$.

3. Results

3.1. Preparation and characterization of PL micelles

MPEG-PCL copolymer was synthesized by ring-opening polymerization of ε-CL on MPEG. The molecular weight determined by ^1H-NMR of the prepared amphiphilic copolymer was 4000 (PEG/PCL = 2000/2000). As shown in Fig. 1A and B, PL micelles were successfully prepared by a one-step solid dispersion method with a ratio 1/19 (PL/copolymer).The average size of PL micelles was 33.2 ± 0.4 nm, with polydispersity index (PDI) of 0.14 ± 0.01 and zeta potential of 0.34 ± 0.17 mV (Fig. 1C and D). TEM image of PL micelles shown in Fig. 1E reveals that PL micelles are spherical and homogeneous in aqueous solution, which was in good accordance with the result of the narrow particle size distribution. In addition, the prepared PL micelles can be lyophilized into a powder form without using any adjuvants. The freeze-dried PL micelle powder was kept at 4 °C before use, and the re-dissolved PL micelles are stable and homogeneous in water. Furthermore, DL and EE of PL micelles were 5.0 ± 0.1% and 99.9 ± 2.7%, respectively.

3.2. In vitro drug release behavior

To investigate the drug release behavior of free PL and PL micelles *in vitro*, a modified dialysis method was employed. As shown in Fig. 1F, PL micelles showed a much slower cumulative release rate when compared with the fast release profile of free PL. Approximately 90% of the PL was released to the media in free PL group within 24 h, whereas only 17% of the encapsulated PL was released from PL micelles. In four days period, the cumulative release rate in PL micelles group (17.42 ± 6.05%) was much lower than that in free PL group (89.78 ± 10.00%, $p < 0.01$). The controlled release profile of PL from the PL micelles indicates its potential applicability as a drug delivery system with elongated blood circulation time and increased accumulation of the therapeutic drug in the tumor site by EPR effect.

3.3. Cytotoxicity, apoptosis induction, and cellular uptake of PL micelles

Cytotoxicity of free PL and PL micelles was determined by MTT on CT-26 cells. According to Fig. 2, both free PL and PL micelles inhibited the growth of CT-26 cells in a dose-dependent manner. Half maximal inhibitory concentration (IC_{50}) of PL micelles (7.10 ± 0.07 μM) was lower than that of free PL (9.98 ± 0.06 μM, $p < 0.05$). Compared with free PL, PL micelles exhibited higher cytotoxicity to CT-26 cells at the same dose of free PL. Meanwhile, cytotoxicity of MPEG-PCL copolymer was also investigated on CT-26 cells, and the results were shown in Fig. 2B, increased concentration of MPEG-PCL copolymer decreased the viability of CT-26 cells, but the cell viabilities were higher than 70%, when the concentration of MPEG-PCL copolymer was up to 10 mg/mL. These results indicated that the MPEG-PCL copolymer showed low cytotoxicity and could serve as a safe anticancer carrier.

FCM analysis was used to investigate apoptosis induced by free PL and PL micelles on CT-26 cells. Early apoptotic cells (Annexin V^+, PI^-) and late apoptotic (Annexin V^+, PI^+) were both counted, and the percent of apoptotic cells in each group were calculated with the apoptotic percent normalized to 5% in control medium DMSO. In Fig. 2C, PL micelles ($18.40 \pm 0.08\%$) induced a stronger apoptosis than free PL ($13.45 \pm 1.37\%$, $p < 0.05$), blank micelles ($4.61 \pm 0.32\%$, $p < 0.05$) and DMSO ($4.98 \pm 0.24\%$, $p < 0.05$).

Given that the enhanced cytotoxicity is often associated with improved cellular uptake, cellular uptake studies of PL micelles and free PL were performed on CT-26 cells at different time intervals.[42] Data in Fig. 2D showed that an increased PL accumulation was observed in cells treated with PL micelles (0.17 ± 0.01 μg/5×10^5 cells) compared with cells treated with free PL (0.13 ± 0.01 μg/5×10^5 cells, $p < 0.01$) at 4 h, but there was no obvious difference between PL micelles and free PL treated groups at 24 h ($p > 0.05$). This result may be due to the viability of cells at 4 h is much better than 24 h when cells have been exposed to PL for 24 h. Uptake of cells may decrease in a time-dependent manner, and the difference between two groups turns smaller over time. These results indicate that encapsulation of PL into MPEG-PCL micelles enhances the uptake of PL into cells to increase the cytotoxic efficacy of the PL at an early stage.

3.4. Modulation of GSH and GSSG

PL can lead to a decrease in GSH levels and an increase in GSSG levels in cancer cells, which contribute to cell apoptosis.[1] Therefore, we examined the effect of PL and PL micelles on GSH and GSSS levels in CT-26 cells using a GSH/GSSG detection kit. Treatment with PL micelles (11.16 ± 0.43 in GSSG level and 0.06 ± 0.05 in GSH level) and free PL (4.30 ± 0.23 in GSSG level and 4.07 ± 0.10 in GSH level) increased GSSG levels and decrease GSH levels compared with blank micelles (1.71 ± 0.04 in GSSG level and 9.50 ± 0.43 in GSH level), and PL micelles showed a more pronounced effect on decreasing GSH levels and increasing GSSG levels in CT-26 cells than free PL ($p < 0.01$). As shown in Fig. 3A and B, PL-mediated GSH depletion was increased by PL micelles sharply, whereas, GSSG levels in PL micelles treated group were higher than free PL treated group.

3.5. Determination of ROS accumulation

We subsequently determined the effect of free PL and PL micelles on cellular ROS levels in CT-26 cancer cells through flow cytometry using the redox-sensitive fluorescent probe DCF-DA. Treatment with PL micelles (10 μM) (1.79 ± 0.09) and free PL (10 μM) (1.51 ± 0.13) for 24 h caused a significant increase in ROS levels in these cancer cells compared with blank micelles (1.01 ± 0.01, $p < 0.05$) and NS (1.00 ± 0.02, $p < 0.05$) group (Fig. 3C). In addition, PL micelles showed a greater increase in the accumulation of ROS level in CT-26 cells than PL-treated groups ($p < 0.05$). Increased ROS levels is often associated with cell apoptosis, PL targeting the stress response to ROS can selectively kill cancer cells.[1] Thus, PL micelles were more potent in inducing tumor cell apoptosis by increasing ROS levels in CT-26 cells.

3.6. PL micelles inhibited proliferation, migration, invasion, and tube formation of HUVECs

To assess the antiangiogenic activity of free PL and PL micelles *in vitro*, their inhibitory effects on VEGF-induced proliferation of HUVECs were measured by MTT assay. As shown in Fig. 4A, both PL micelles and free PL significantly inhibited proliferation of HUVECs and PL micelles showed a lower IC$_{50}$ (4.51 ± 0.12 μM) than free PL (8.02 ± 0.44 μM, $p < 0.05$).

Migration and invasion are essential for endothelial cells in angiogenesis. We conducted wound healing assays to evaluate the effects of free PL and PL micelles on cell migration. The migrated HUVECs were quantified by manual counting, and result was expressed as percentage of inhibition using untreated cells as 100%. In Fig. 4B, we found that both free PL and PL micelles inhibited migration of HUVECs (Fig. 4E), and PL micelles ($21.67 \pm 2.40\%$) showed a stronger inhibitory effect than free PL ($42.33 \pm 2.60\%$, $p < 0.01$).

We also conducted transwell invasion assays to investigate the ability of HUVECs to pass through the Matrigel and membrane barrier of the transwell in the presence of blank micelles, free PL, or PL micelles. Data (Fig. 4C and F) showed that PL micelles ($2.00 \pm 1.51\%$) exhibit a stronger inhibitory effect on invasion properties of endothelial cells than free PL ($34.00 \pm 4.04\%$, $p < 0.01$)

Processes of several kinds of cells were involved in angiogenesis, among which tube formation of endothelial cells is one of the critical steps. In NS and blank micelles group, HUVECs plated on the surface of Matrigel formed capillary-like structures within 6 h. However, treatment with free PL and PL micelles inhibited the tube formation (Fig. 4D and G) and PL micelles (1.67 ± 0.67) induced a stronger inhibitory effect than free PL (25.00 ± 3.46, $p < 0.05$).

As shown in Fig. 4, results indicated that both free PL and PL micelles had anti-angiogenic efficacy in migration, invasion, and tube formation of HUVECs, and PL micelles showed a stronger anti-angiogenic efficacy than free PL.

3.7. PL micelles inhibited embryonic angiogenesis in transgenic zebrafish model

Transgenic zebrafish and their embryos have been utilized in pharmacological research and drug discovery processes.[43] To elucidate whether PL micelles enhance the anti-angiogenesis effects we carried out the comparison study of free PL and PL micelles in transgenic zebrafish embryos. Briefly, 15 hpf zebrafish embryos were incubated with free PL, PL micelles, blank micelles and DMSO (0.1%) for the next 15 h. Then, zebrafish embryos were anesthetized with 0.01% tricaine, and digital images of each embryo were captured by a fluorescence microscope. Free PL and PL micelles treatments significantly inhibited the intersegmental blood vessel growth compared

with blank micelles and DMSO (0.1%) treated embryos (Fig. 5A). Length of intersegmental vessels (ISVs) in PL micelles group (21.67 ± 1.20 μm) was shorter than that in free PL (32.33 ± 1.45 μm, $p < 0.01$), blank micelles (56.67 ± 2.40 μm, $p < 0.01$), or DMSO (55.33 ± 0.88 μm, $p < 0.01$) group (Fig. 5B). Results suggested that PL micelles enhance the anti-angiogenesis effect of free PL in zebrafish.

3.8. Alginate-encapsulated tumor cell assay

In order to further investigate the anti-angiogenesis effect of PL micelles, an alginate-encapsulated tumor cell assay was also employed to evaluate the inhibitory activity of PL micelles on angiogenesis *in vivo*. Compared with blank micelles and NS group, new blood vessels in alginate beads from free PL and PL micelles-treated mice were remarkably sparse (Fig. 6A, B, C, D). Meanwhile, as shown in Fig. 6F, uptake of FITC-dextran in PL micelles group (0.98 ± 0.07 μg/bead) was lower than that of free PL (1.94 ± 0.08 μg/bead, $p < 0.01$), blank micelles (3.16 ± 0.11 μg/bead, $p < 0.01$), or NS group (3.14 ± 0.15 μg/bead, $p < 0.01$). The results presented above indicated that PL micelles significantly inhibited tumor angiogenesis, which participated in suppression of tumor growth and metastasis.

3.9. In vivo anti-tumor activity

Subcutaneous murine CT-26 colon tumor model was used to assay the anti-tumor activity of PL micelles. Compared with free PL group, PL micelles was more efficient in suppressing tumor growth, whereas blank micelles show no anti-tumor activity (Fig. 7A-C). As shown in Fig. 7B, tumor weight in PL micelles group (0.87 ± 0.27 g) was significantly lower than that in free PL (3.00 ± 0.59 g, $p < 0.05$), blank micelles (4.15 ± 0.57, $p < 0.01$), or NS group (3.29 ± 0.53 g, $p < 0.05$). Besides, tumor volume in PL micelles group were significantly smaller than in free PL, blank micelles and NS treated group ($p < 0.05$). Furthermore, substantial increase in the life span of the PL micelles-treated mice was observed. PL micelles prolonged the survival time of tumor bearing mice compared with free PL, blank micelles, and NS group, respectively (Fig. 7D). These results indicated that PL micelles were efficient in inhibiting growth of implanted tumors and prolonging survival time of CT-26 tumor bearing mice.

As shown in Fig. 7F, body weight of mice in free PL and PL micelles treated

groups were less than that in NS and blank micelles treated groups. This observation can be attributed to more increased weight of tumor tissues in NS and blank micelles treated mice than that in free PL and PL micelles treated groups. In addition, no apparent toxicities such as depressed hair quality, splenomegaly or other organ damage were observed in PL micelles treated mice during the experimental period.

3.10. MVD determination

As shown in Fig. 8, immunohistochemical anti-CD31 staining of the tumor tissue from mice in each group revealed that PL micelles significantly decreased MVD compared with free PL, blank micelles and NS group. In Fig. 8F, MVD of tumor tissues from PL micelles-treated mice (11.80 ± 1.24) was significantly lower compared with free PL (20.40 ± 1.08, $p < 0.01$), blank micelles (47.60 ± 1.60, $p < 0.01$), or NS group (46.60 ± 1.36, $p < 0.01$). PL micelles showed a stronger anti-angiogenesis effect than free PL both *in vitro* and *in vivo.*

3.11. Quantitative assessment of apoptosis

We next analyzed the effect of PL micelles on apoptosis in tumors by TUNEL staining. TUNEL positive cells were counted only in regions of intact tumor, in such a way that the central necrosis observed did not interfere with the quantification of apoptotic cells. Representative fields of each group were shown, which clearly indicated more apoptotic tumor cells in mice treated with PL micelles and free PL. Besides, PL micelles-treated group showed a more pronounced apoptosis than free PL group. The number of TUNEL positive cells in 5 random fields from 3 different tumors in each group was counted manually, and the apoptotic index is shown in Fig. 9. The number of TUNEL positive cells was significantly higher in PL micelles group (18.39 ± 0.78) than in free PL (13.45 ± 1.37, $p < 0.01$), blank micelles (4.61 ± 0.33, $p < 0.01$), or NS group (4.98 ± 0.24, $p < 0.01$), respectively (Fig. 9E).

3.12. Determination of tumor cell proliferation

Proliferation of tumor cells was examined by immunohistochemical staining of Ki-67. As shown in Fig. 10A to D, within a similar high-power field, less Ki-67 positive cells in tumor tissues were observed in PL micelles-treated group compared with free PL, blank micelles, or NS group. The number of Ki-67 positive cells was

significantly lower in PL micelles group (14.33 ± 2.33%) than in free PL (28.67 ± 1.20%, p < 0.01), blank micelles (71.00 ± 2.31%, p < 0.01), or NS group (70.33 ± 1.45%, p < 0.01), respectively (Fig. 10E).

4. Discussion

PL is a promising compound for cancer therapy, which can selectively kill cancer cells by targeting the stress response to ROS irrespective of normal cells.[1] Efforts concerning the preparation of water-based formulation of PL have been made to improve the antitumor activity of PL *in vivo*. In previous reports, PL loaded PEG-β-PDAEMA nanoparticles exhibit superior efficacy in impeding the tumor growth compared to free PL.[44] In this study, we encapsulate PL into MPEG-PCL copolymer which showed excellent properties in particle size, EE, DL, stability, and *in vitro* and *in vivo* anti-tumor activity.[42] Compared with previously reported PL/PEG-β-PDAEMA nanoparticles, PL micelles in our work have much advantages, such as small size (33.2 nm *vs.* 109.0 nm), high encapsulation efficiency (99.9 ± 2.7% *vs.* 67.0 ± 3.0%), simple one step preparation method, and good re-solubility. Therefore, PL micelles may have applications as a potent intravenous formulation of PL for cancer therapy.

Several investigations concerning the anti-tumor activity of PL micelles were made in our study. PL encapsulated in MPEG-PCL copolymer showed stronger antitumor activity than free PL both *in vitro* and *in vivo.* In the *in vitro* tests, PL micelles showed an increased cytotoxicity and induction of apoptosis in CT-26 cells compared with free PL, and there was no difference between blank micelles-treated and control groups. Besides, in the *in vivo* tests, PL micelles were more efficient in inhibiting tumor growth, and prolonging the survival of tumor-bearing mice compared with free PL in a subcutaneous murine CT-26 tumor model, which was confirmed by CD31, TUNEL and Ki-67 staining of tumor tissues. Subsequently, cellular uptake studies were carried out, and the result suggested that the higher cytotoxicity of the PL micelles was associated with their enhanced uptake in cells. Compared with free PL in Fig. 1F, the much slower release behavior of PL from MPEG-PCL micelles can be attributed to the ''core-shell'' structural characteristics of polymeric micelles.

ROS, in normal conditions, are important in signal transduction and gene transcription. However, increase of ROS amounts in cancer cells by PL binding to the active sites of key cellular antioxidants including glutathione S transferase and carbonyl reductase 1 can lead to death of cancer cell.[1, 45] PL could not raise ROS levels in normal cells because of the lower quantity of antioxidants due to less activity of Nrf2 (NF-E2-related factor 2) transcription factor.[46] To test weather PL micelles could interfere with ROS levels in cancer cells, we carried out our experiment on CT-26 cells. Both free PL and PL micelles induced an increase in ROS levels and a higher cellular ROS levels was observed in PL micelles-treated CT-26 cells. The elevated levels of ROS should contribute to the increased apoptosis of cancer cells. In addition, a much lower cellular GSH level and a significant higher GSSG level were observed in PL micelles treated group compared with free PL treated groups, as shown in Fig. 3. The sharply depleted cellular GSH and increased GSSG level should be a result of PL binding to glutathione S transferase.

Neovascularization plays an essential role in the growth of tumors. The new blood vessels grow and infiltrate into the tumors, providing them with essential nutrients and oxygen, and a route for tumor metastasis. PL was proved to be effective in anti-angiogenesis, which was confirmed by alginate-encapsulated tumor cell assay in our study, and PL micelles inhibited the growth of tumor blood vessels more remarkably than free PL. Besides, the significantly decreased MVD in CD 31 staining of tumor tissue in PL micelles treated mice compared with free PL indicate that encapsulate PL into MPEG-PCL copolymer improves the anti-angiogenesis efficiency of PL. Generation of ROS is considered to hamper efficient cell migration in wound healing, which is essential in neovascularization.[47] In order to further investigate the inhibitory effect of PL micelles on tumor neovascularization, experiment on HUVECs proliferation, migration, invasion, and tube formation were performed. Data reveal that PL micelles are more potent in inhibiting HUVEC proliferation, migration, invasion, and tube formation than free PL. In zebrafish model, length of ISVs in PL micelles group was shorter than that in free PL, providing that PL micelles were more effective than free PL in inhibiting neovascularization.

5. Conclusions

Biodegradable PL micelles were prepared and assigned for therapy of colon carcinoma both *in vitro* and *in vivo*. PL micelles exhibited increased cellular uptake, cytotoxicity and anti-angiogenesis effect *in vitro* compared with free PL. Encapsulation of PL into polymeric micelles could increase the cytotoxicity, cellular uptake, ROS and GSSG, and reduce GSH levels *in vitro*. In transgenic zebrafish model, PL micelles inhibited both embryonic angiogenesis and tumor-induced angiogenesis. Furthermore, compared with free PL, PL micelles were more effective in suppressing tumor growth and prolonged survival in the mouse models. The PL micelles prepared in this work thus may enable application in colon carcinoma therapy.

Declaration of Interest statement

The authors report no conflicts of interest. The authors alone are responsible for the content and writing of the paper.

References

1. L. Raj, T. Ide, A. U. Gurkar, M. Foley, M. Schenone, X. Li, N. J. Tolliday, T. R. Golub, S. A. Carr and A. F. Shamji, *Nature*, 2011, **475**, 231-234.
2. P. T. Schumacker, *Cancer cell*, 2006, **10**, 175-176.
3. D. Trachootham, Y. Zhou, H. Zhang, Y. Demizu, Z. Chen, H. Pelicano, P. J. Chiao, G. Achanta, R.

B. Arlinghaus and J. Liu, *Cancer cell*, 2006, **10**, 241-252.

4.   S. Hansen, D. A. Grabau, F. B. Sørensen, M. Bak, W. Vach and C. Rose, *Clin. Cancer Res.*, 2000, **6**, 139-146.

5.   Q. J. Wu, C. Y. Gong, S. T. Luo, D. M. Zhang, S. Zhang, H. S. Shi, L. Lu, H. X. Yan, S. S. He and D. D. Li, *BMC cancer*, 2012, **12**, 129.

6.   M. S. Butler, *J. Nat. Prod.*, 2004, **67**, 2141-2153.

7.   D. J. Newman and G. M. Cragg, *J. Nat. Prod.*, 2007, **70**, 461-477.

8.   M. J. Balunas and A. D. Kinghorn, *Life Sci.*, 2005, **78**, 431-441.

9.   D. P. Bezerra, G. C. G. Militão, F. O. De Castro, C. Pessoa, M. O. De Moraes, E. R. Silveira, M. A. S. Lima, F. J. M. Elmiro and L. V. Costa-Lotufo, *Toxicol. in vitro*, 2007, **21**, 1-8.

10.   C. Bernard, H. Krishanmurty, D. Chauret, T. Durst, B. Philogene, P. Sanchez-Vindas, C. Hasbun, L. Poveda, L. San Román and J. Arnason, *J. Chem. Ecol.*, 1995, **21**, 801-814.

11.   P. Srinivasa Reddy, K. Jamil, P. Madhusudhan, G. Anjani and B. Das, *Pharm. Bio.*, 2001, **39**, 236-238.

12.   B. S. Park, D. J. Son, W. S. Choi, G. R. Takeoka, S. O. Han, T. W. Kim and S. E. Lee, *Phytother. Res.*, 2008, **22**, 1195-1199.

13.   K. V. Golovine, P. B. Makhov, E. Teper, A. Kutikov, D. Canter, R. G. Uzzo and V. M. Kolenko, *The Prostate*, 2013, **73**, 23-30.

14.   D. P. Bezerra, C. Pessoa, M. O. d. Moraes, N. Alencar, R. O. Mesquita, M. W. Lima, A. P. N. Alves, O. D. L. Pessoa, J. H. Chaves and E. R. Silveira, *J. Appl. Toxicol.*, 2008, **28**, 599-607.

15.   S. W. Lee and A. Mandinova, Google Patents, 2009.

16.   M. Jarvius, M. Fryknäs, P. D'Arcy, C. Sun, L. Rickardson, J. Gullbo, C. Haglund, P. Nygren, S. Linder and R. Larsson, *Biochem. Bioph. Res. Co.*, 2013, **431**, 117-123.

17.   D. J. Adams, M. Dai, G. Pellegrino, B. K. Wagner, A. M. Stern, A. F. Shamji and S. L. Schreiber, *PNAS*, 2012, **109**, 15115-15120.

18.   L. Zhang, J. M. Chan, F. X. Gu, J.-W. Rhee, A. Z. Wang, A. F. Radovic-Moreno, F. Alexis, R. Langer and O. C. Farokhzad, *ACS Nano.*, 2008, **2**, 1696-1702.

19.   V. Wagner, A. Dullaart, A.-K. Bock and A. Zweck, *Nat. Biotechnol.*, 2006, **24**, 1211-1218.

20.   K. Hennenfent and R. Govindan, *Ann. Oncol.*, 2006, **17**, 735-749.

21.   G. Zhang, X. Zeng and P. Li, *J. Biomed. Nanotechnol.*, 2013, **9**, 741-750.

22.   C. Gong, X. Wei, X. Wang, Y. Wang, G. Guo, Y. Mao, F. Luo and Z. Qian, *Nanotechnology*, 2010, **21**, 215103.

23.   C. Gong, Y. Wang, X. Wang, X. Wei, Q. Wu, B. Wang, P. Dong, L. Chen, F. Luo and Z. Qian, *J. Nanopart. Res.*, 2011, **13**, 721-731.

24.   C. Gong, C. Wang, Y. Wang, Q. Wu, D. Zhang, F. Luo and Z. Qian, *Nanoscale*, 2012, **4**, 3095-3104.

25.   L. Lv, Y. Shen, M. Li, X. Xu, M. Li, S. Guo and S. Huang, *J. Biomed. Nanotechnol.*, 2014, **10**, 324-335.

26.   Q. Guo, X. Li, Y. Yang, J. Wei, Q. Zhao, F. Luo and Z. Qian, *J. Biomed. Nanotechnol.*, 2014, **10**, 227-237.

27.   Y.-A. Shieh, S.-J. Yang, M.-F. Wei and M.-J. Shieh, *ACS Nano.*, 2010, **4**, 1433-1442.

28.   T. G. Shutava, S. S. Balkundi, P. Vangala, J. J. Steffan, R. L. Bigelow, J. A. Cardelli, D. P. O'Neal and Y. M. Lvov, *ACS Nano.*, 2009, **3**, 1877-1885.

29.   M. Gou, K. Men, J. Zhang, Y. Li, J. Song, S. Luo, H. Shi, Y. Wen, G. Guo and M. Huang, *ACS*

Nano., 2010, **4**, 5573-5584.

30. J. Fang, H. Nakamura and H. Maeda, *Adv. Deliver. Rev.*, 2011, **63**, 136-151.

31. P. H.-L. Tran, T. T.-D. Tran and B.-J. Lee, *J. Biomed. Nanotechnol.*, 2014, **10**, 154-165.

32. N. Aher, S. Banerjee, S. Bhansali, R. Yadav, M. Shidore, S. Mhaske, R. Chaudhari, S. Asai, A. Jalota-Badhwar and J. Khandare, *J. Biomed. Nanotechnol.*, 2013, **9**, 776-789.

33. E. A. Jaffe, R. L. Nachman, C. G. Becker and C. R. Minick, *J. Clin. Invest.*, 1973, **52**, 2745.

34. C. Gong, S. Shi, P. Dong, B. Kan, M. Gou, X. Wang, X. Li, F. Luo, X. Zhao and Y. Wei, *Int. J. Pharm.*, 2009, **365**, 89-99.

35. D. S. Heo, J.-G. Park, K. Hata, R. Day, R. B. Herberman and T. L. Whiteside, *Cancer Res.*, 1990, **50**, 3681-3690.

36. C. Timke, H. Zieher, A. Roth, K. Hauser, K. E. Lipson, K. J. Weber, J. Debus, A. Abdollahi and P. E. Huber, *Clin. Cancer Res.*, 2008, **14**, 2210-2219.

37. X. Pang, Z. Yi, X. Zhang, B. Sung, W. Qu, X. Lian, B. B. Aggarwal and M. Liu, *Cancer Res.*, 2009, **69**, 5893-5900.

38. C. B. Kimmel, W. W. Ballard, S. R. Kimmel, B. Ullmann and T. F. Schilling, *Dev. Dynam.*, 1995, **203**, 253-310.

39. J. Hoffmann, M. Schirner, A. Menrad and M. R. Schneider, *Cancer Res.*, 1997, **57**, 3847-3851.

40. P. Blezinger, J. Wang, M. Gondo, A. Quezada, D. Mehrens, M. French, A. Singhal, S. Sullivan, A. Rolland and R. Ralston, *Nat. Biotechnol.*, 1999, **17**, 343-348.

41. J. Halder, A. A. Kamat, C. N. Landen, L. Y. Han, S. K. Lutgendorf, Y. G. Lin, W. M. Merritt, N. B. Jennings, A. Chavez-Reyes and R. L. Coleman, *Clin. Cancer Res.*, 2006, **12**, 4916-4924.

42. C. Gong, Y. Xie, Q. Wu, Y. Wang, S. Deng, D. Xiong, L. Liu, M. Xiang, Z. Qian and Y. Wei, *Nanoscale*, 2012, **4**, 6004-6017.

43. L. I. Zon and R. T. Peterson, *Nat. Rev. Drug Discov.*, 2005, **4**, 35-44.

44. J. Wang, K. Yao, C. Wang, C. Tang and X. Jiang, *J. Mater. Chem. B*, 2013, **1**, 2324-2332.

45. S. Saeidnia and M. Abdollahi, *Toxicol. Appl. Pharm.*, 2013.

46. D. J. Burgess, *Nat. Rev. Drug Discov.*, 2011, **10**, 658-659.

47. Z. Zhou, S. Joslin, A. Dellinger, M. Ehrich, B. Brooks, Q. Ren, U. Rodeck, R. Lenk and C. L. Kepley, *J. Biomed. Nanotechnol.*, 2010, **6**, 605-611.

Figure Legends

Fig.1 Preparation and characterization of PL micelles. A: Chemical structure of PL; B: Preparation scheme of PL micelles; C: Particle size distribution of PL micelles; D: zeta potential of PL micelles; E: TEM image of PL micelles; F: Drug release profile of free PL and PL micelles in PBS solution at pH 7.4 with error bars representing the standard deviation (n =5), **p < 0.01 *vs.* free PL.

Fig.2 Cytotoxicity studies and cellular uptake assay of PL micelles. A: Cytotoxicity studies of PL micelles and free PL on CT-26 cells; B: Cytotoxicity evaluation of MPEG-PCL copolymer on CT-26 cells; C: Induction of apoptosis by PL micelles and free PL on CT-26 cells, * p < 0.05 *vs.* free PL; D: PL accumulation in CT-26 cells, **p < 0.01 *vs.* free PL.

Fig.3 PL micelles modulated GSH and GSSG levels and enhanced ROS accumulation in CT-26 cells. PL micelles (10 μM) mediated modulation of GSH levels (A) and GSSG levels (B), **p < 0.01 vs. free PL; PL (10 μM) induced ROS accumulation (C), *p < 0.05 *vs.* free PL.

Fig.4 PL micelles inhibited proliferation, migration, invasion, and tube formation of HUVECs. A: PL micelles inhibited HUVEC proliferation; B: PL micelles inhibited HUVEC migration in wound healing assay; C: PL micelles inhibited HUVEC invasion; D: PL micelles inhibited tube formation of HUVECs, **p < 0.01 *vs.* free PL; E: Images of HUVEC migration of each group; F: Images of HUVEC invasion of each group; G: Images of tube formation of HUVECs in each group.

Fig.5 PL micelles inhibited embryonic angiogenesis. A: Fluorescent images of 30 hpf zebrafish treated with NS, blank micelles, free PL, and PL micelles. Intersegmental vessels (ISVs) growth was remarkably inhibited in PL micelles group; B: Length of ISVs in embryonic angiogenesis model, **p < 0.01 *vs.* free PL.

Fig.6 Alginate-encapsulated tumor cell assay. Representative images of alginate bead in NS (A), blank micelles (B), free PL (C), and PL micelles (D) group, and uptake of FITC-dextran in each group (E), **p < 0.01 *vs.* free PL.

Fig.7 PL micelles inhibited growth in subcutaneous CT-26 model. A: Representative

photographs of subcutaneous tumors in each group; B: Weight of subcutaneous tumors in each group. C: Suppression of subcutaneous tumor growth by PL micelles in tumor-bearing mice (n=6); D: Survival curve of mice in each group (n=6). E: Body weight of tumor-bearing mice in each group (n=6), *p < 0.05 *vs.* free PL.

Fig.8 CD31 immunohistochemical staining of tumors. Representative CD31 immunohistochemical images of NS (A), blank micelles (B), free PL (C), and PL micelles (D), and MVD in each group (E), **p < 0.01 *vs.* free PL.

Fig.9 TUNEL immunofluorescent staining of tumors. Representative TUNEL immunofluorescent images of NS (A), blank micelles (B), free PL (C), and PL micelles (D) group, and mean apoptotic index in each group (E), **p < 0.01 *vs.* free PL.

Fig.10 Ki-67 immunohistochemical staining of tumors. Representative Ki-67 immunohistochemical images of NS (A), blank micelles (B), free PL (C), and PL micelles (D) group, and mean Ki-67 LI in each group (E), **p < 0.01 *vs.* free PL.
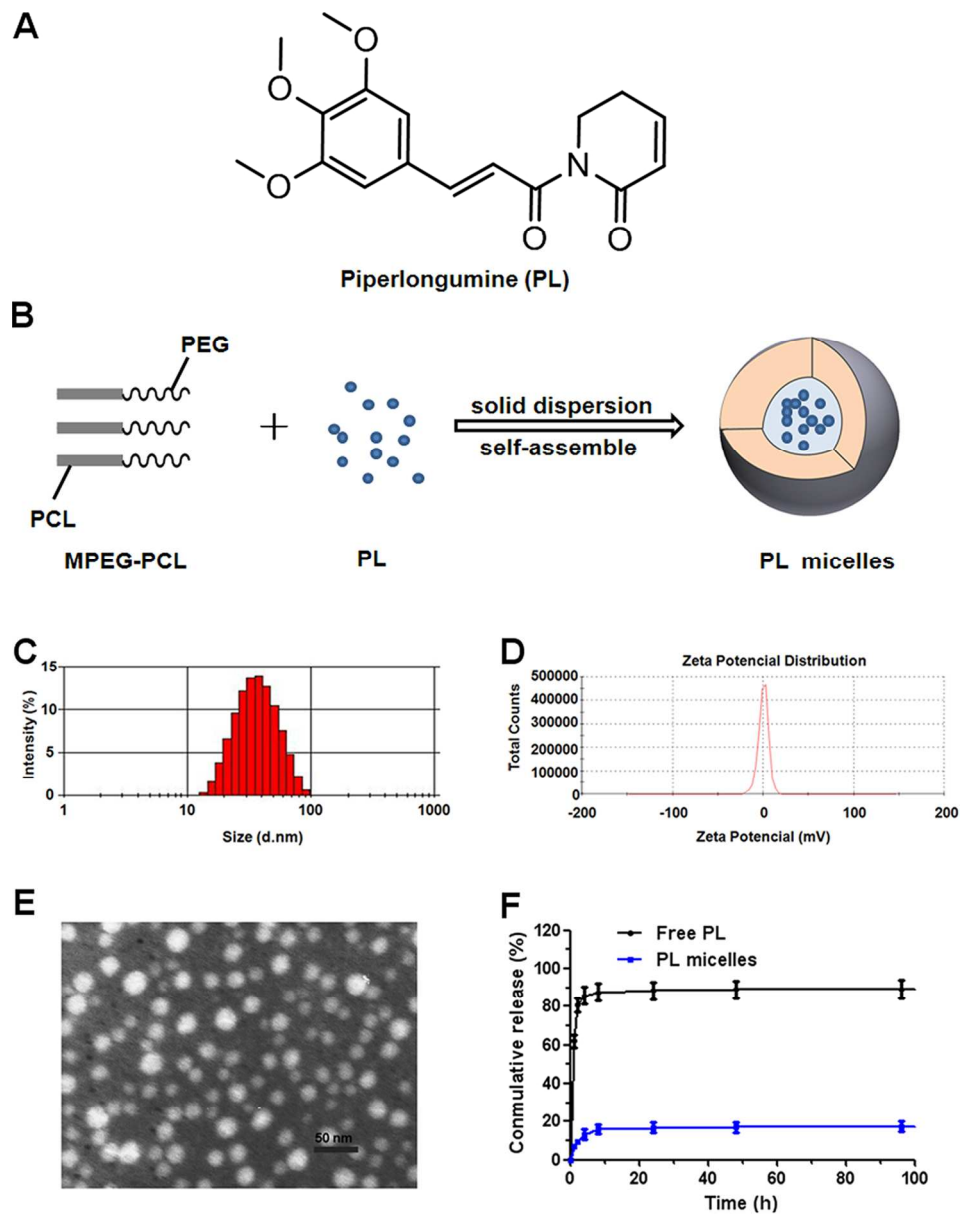
Preparation and characterization of PL micelles. A: Chemical structure of PL; B: Preparation scheme of PL micelles; C: Particle size distribution of PL micelles; D: zeta potential of PL micelles; E: TEM image of PL micelles; F: Drug release profile of free PL and PL micelles in PBS solution at pH 7.4 with error bars representing the standard deviation (n =5), **$p < 0.01$ vs. free PL.
127x160mm (300 x 300 DPI)
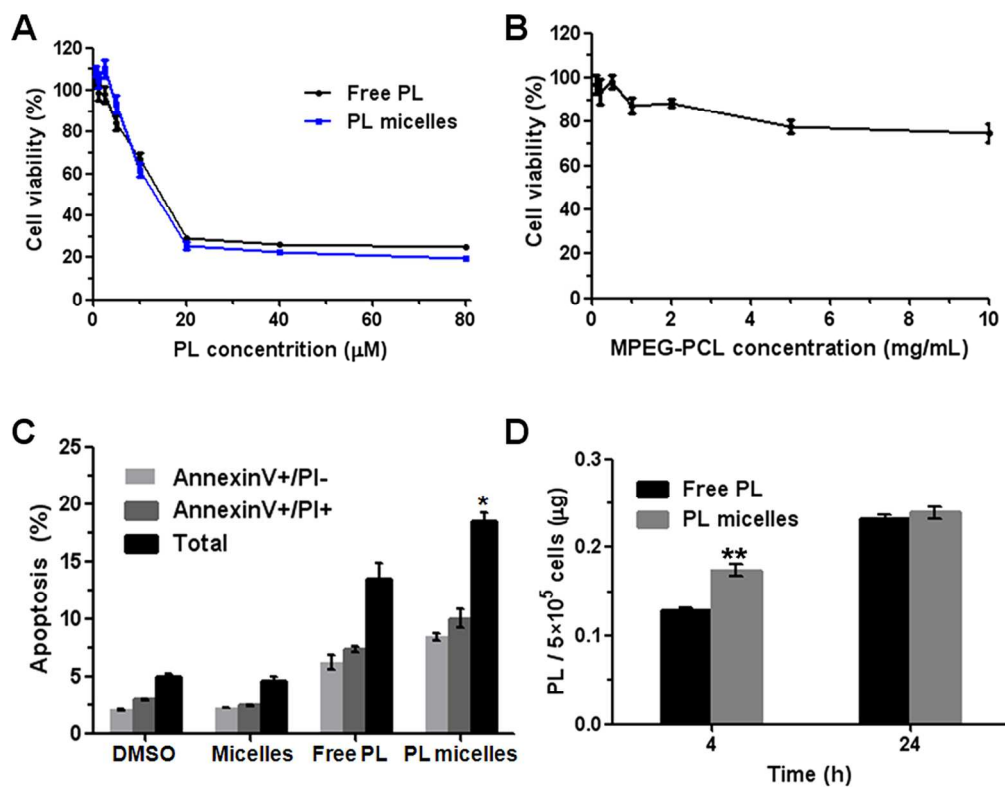
Cytotoxicity studies and cellular uptake assay of PL micelles. A: Cytotoxicity studies of PL micelles and free PL on CT-26 cells; B: Cytotoxicity evaluation of MPEG-PCL copolymer on CT-26 cells; C: Induction of apoptosis by PL micelles and free PL on CT-26 cells, * p < 0.05 vs. free PL; D: PL accumulation in CT-26 cells, **p < 0.01 vs. free PL.
127x98mm (300 x 300 DPI)
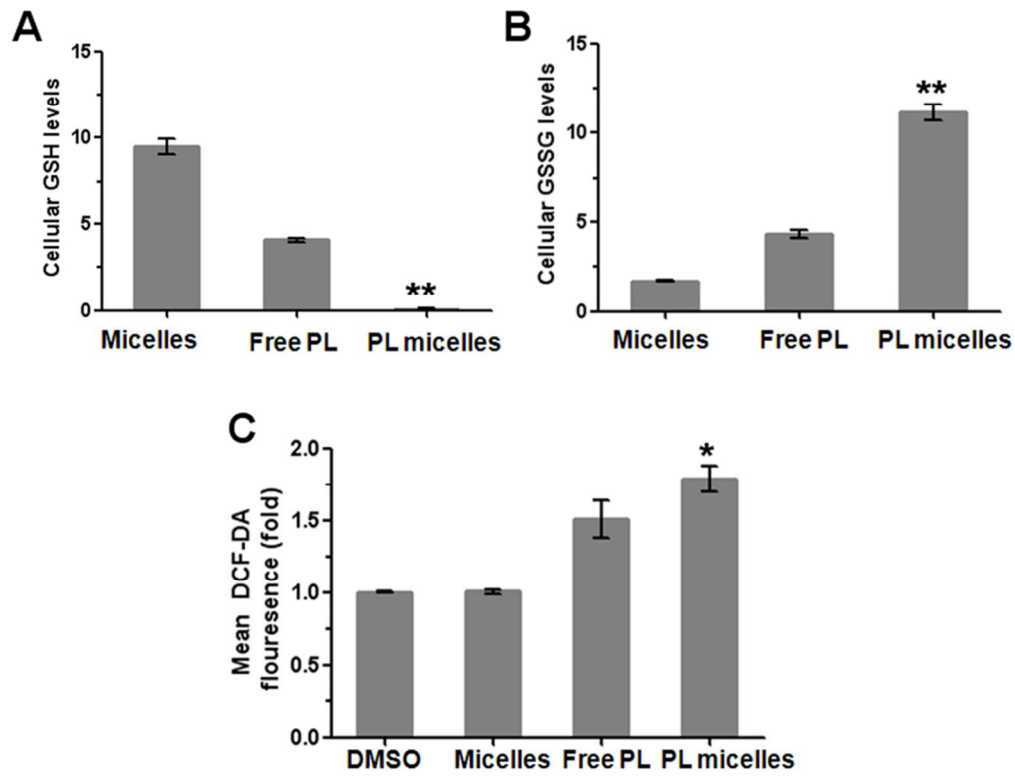
PL micelles modulated GSH and GSSG levels and enhanced ROS accumulation in CT-26 cells. PL micelles (10 μM) mediated modulation of GSH levels (A) and GSSG levels (B), **$p < 0.01$ vs. free PL; PL (10 μM) induced ROS accumulation (C), *$p < 0.05$ vs. free PL
101x77mm (300 x 300 DPI)
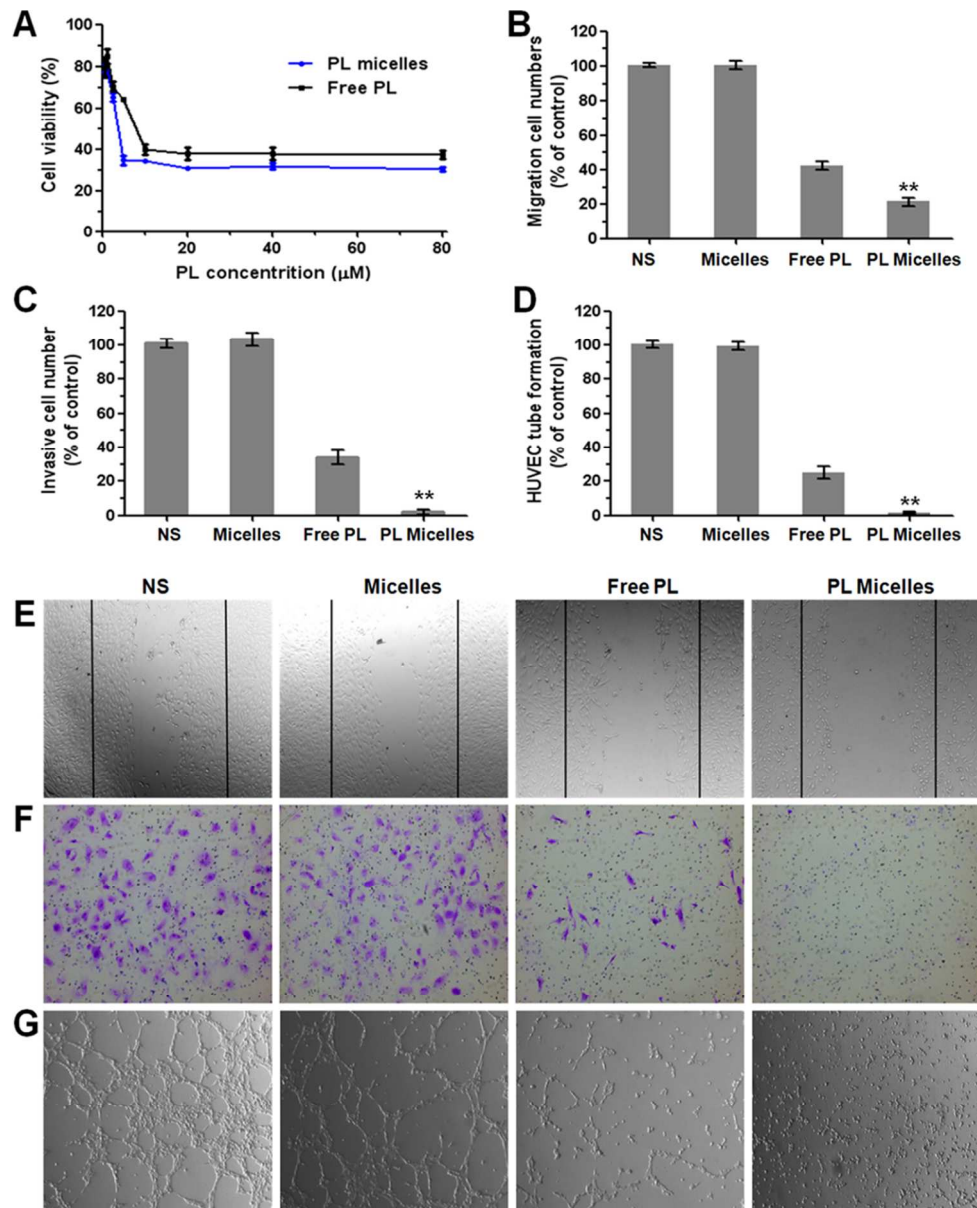
PL micelles inhibited proliferation, migration, invasion, and tube formation of HUVECs. A: PL micelles inhibited HUVEC proliferation; B: PL micelles inhibited HUVEC migration in wound healing assay; C: PL micelles inhibited HUVEC invasion; D: PL micelles inhibited tube formation of HUVECs, **p < 0.01 vs. free PL; E: Images of HUVEC migration of each group; F: Images of HUVEC invasion of each group; G: Images of tube formation of HUVECs in each group.
101x125mm (300 x 300 DPI)
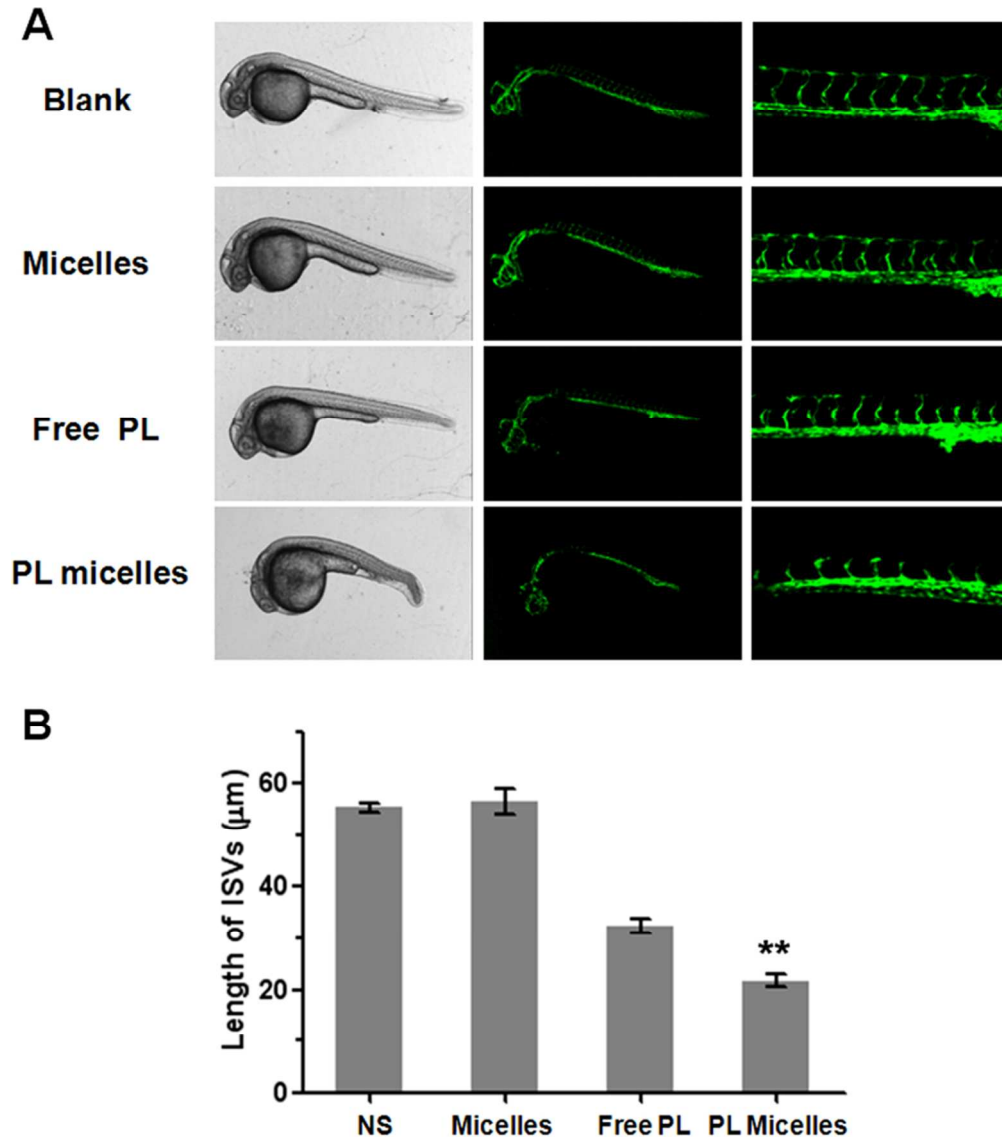
PL micelles inhibited embryonic angiogenesis. A: Fluorescent images of 30 hpf zebrafish treated with NS, blank micelles, free PL, and PL micelles. Intersegmental vessels (ISVs) growth was remarkably inhibited in PL micelles group; B: Length of ISVs in embryonic angiogenesis model, **p < 0.01 vs. free PL.
101x114mm (300 x 300 DPI)
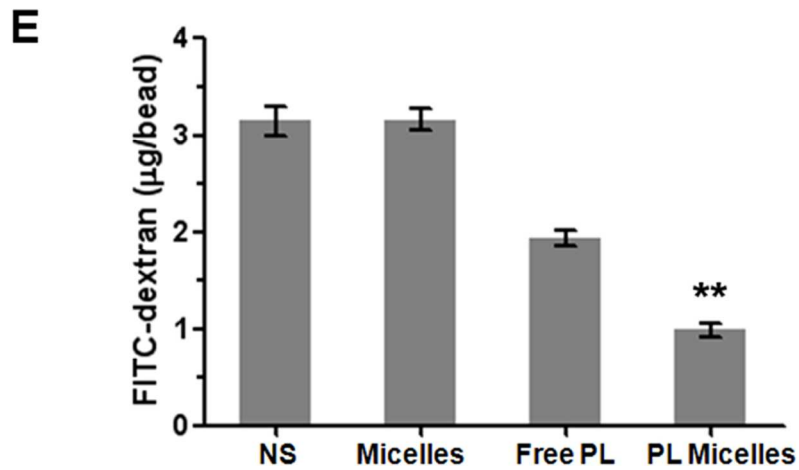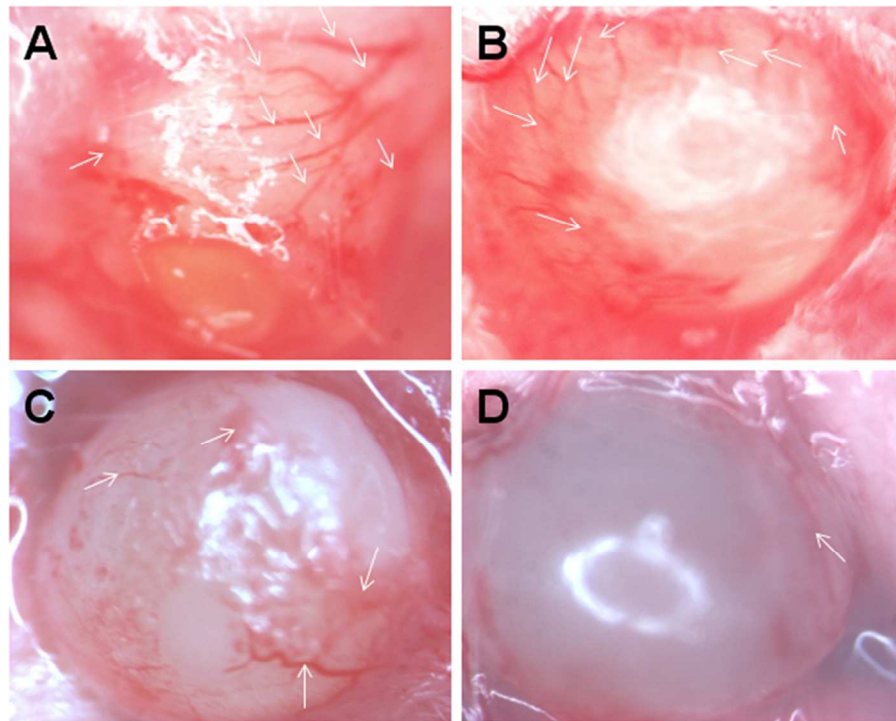
Alginate-encapsulated tumor cell assay. Representative images of alginate bead in NS (A), blank micelles (B), free PL (C), and PL micelles (D) group, and uptake of FITC-dextran in each group (E), **p < 0.01 vs. free PL.
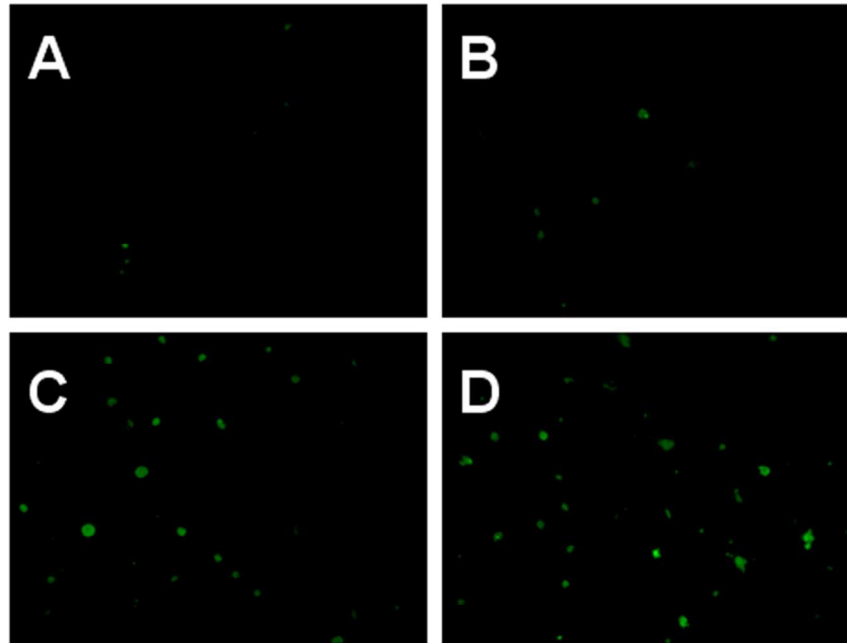101x135mm (300 x 300 DPI)
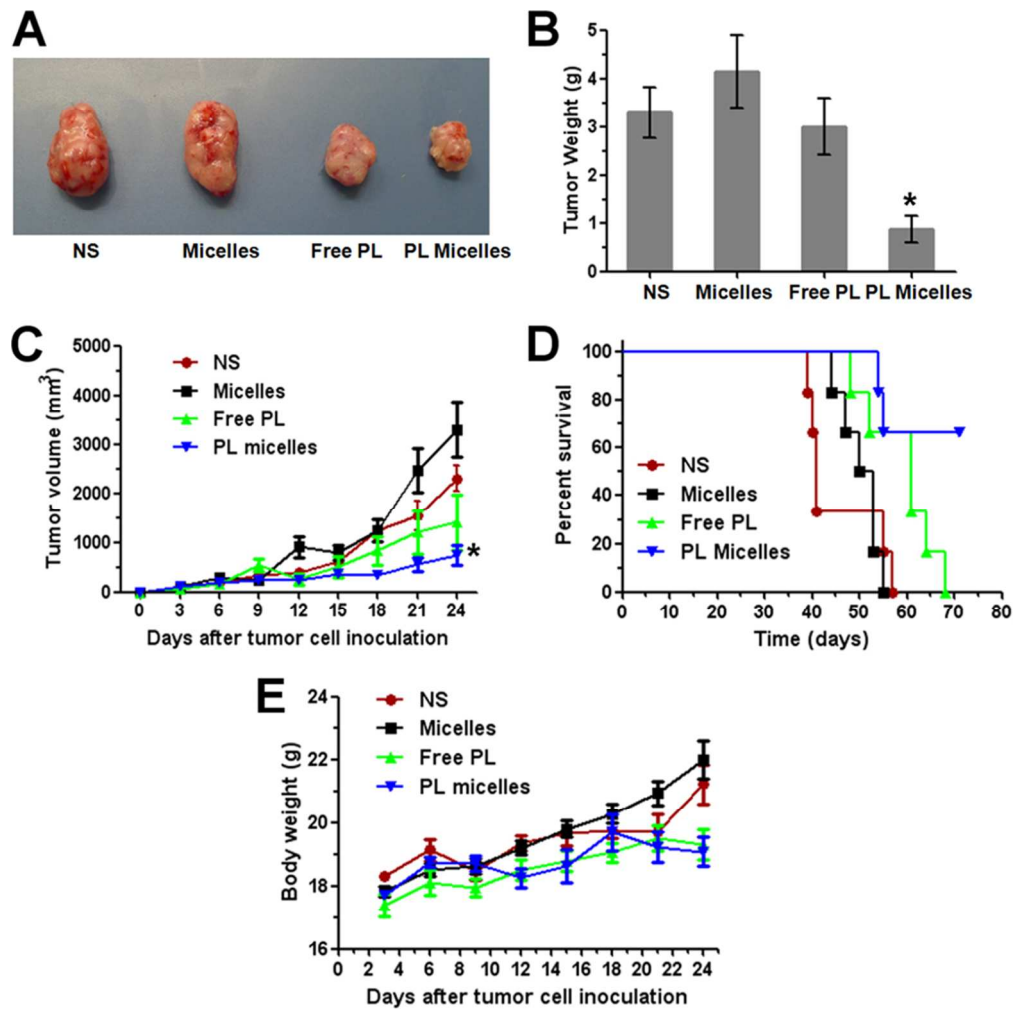
PL micelles inhibited growth in subcutaneous CT-26 model. A: Representative photographs of subcutaneous tumors in each group; B: Weight of subcutaneous tumors in each group. C: Suppression of subcutaneous tumor growth by PL micelles in tumor-bearing mice (n=6); D: Survival curve of mice in each group (n=6). E: Body weight of tumor-bearing mice in each group (n=6), *p < 0.05 vs. free PL.
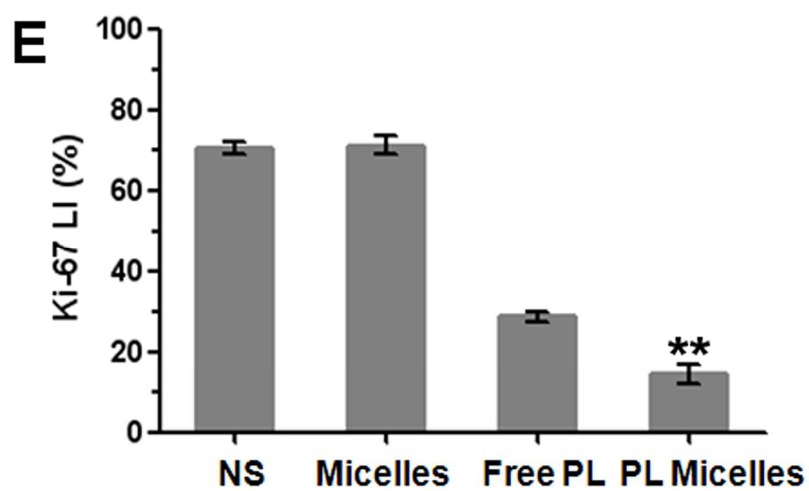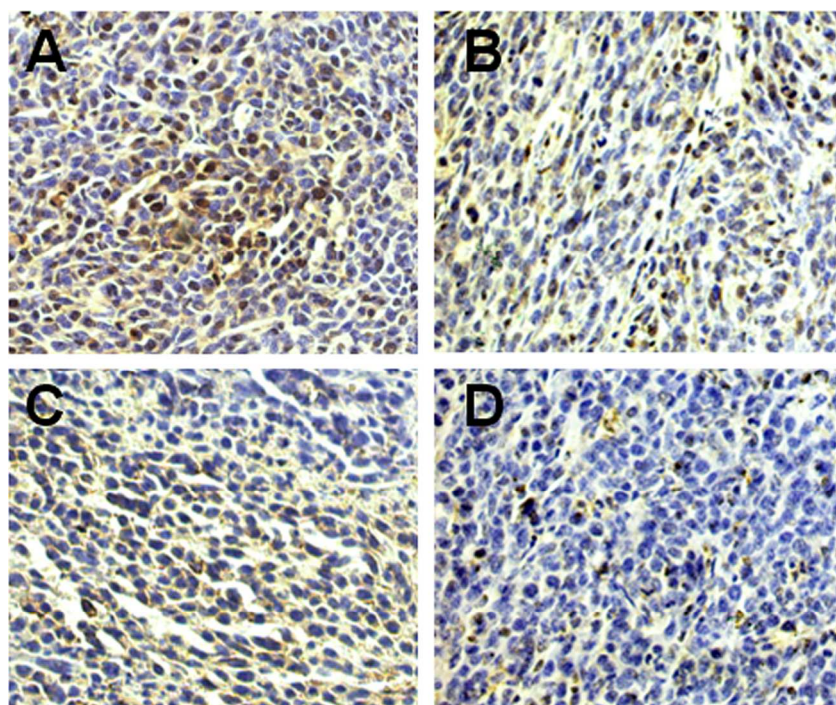101x101mm (300 x 300 DPI)
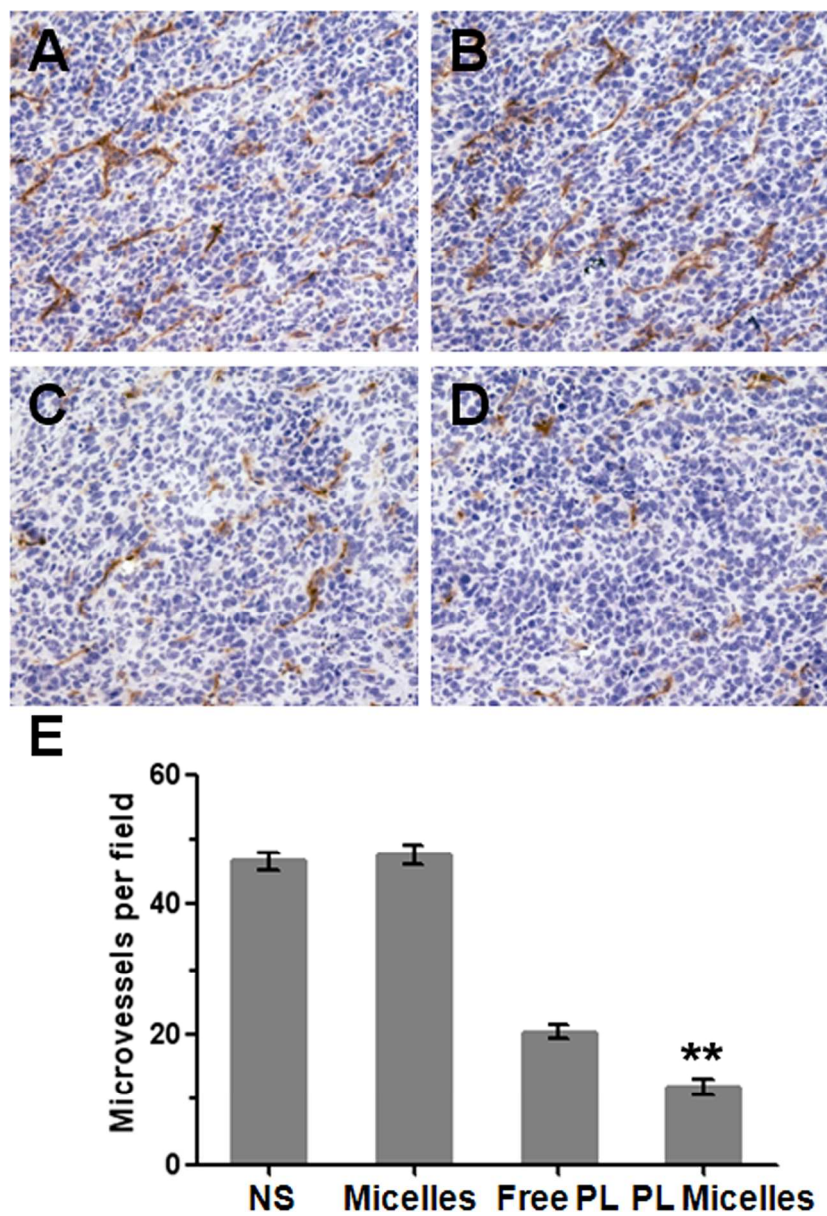
CD31 immunohistochemical staining of tumors. Representative CD31 immunohistochemical images of NS (A), blank micelles (B), free PL (C), and PL micelles (D), and MVD in each group (E), **p < 0.01 vs. free PL.
127x183mm (300 x 300 DPI)
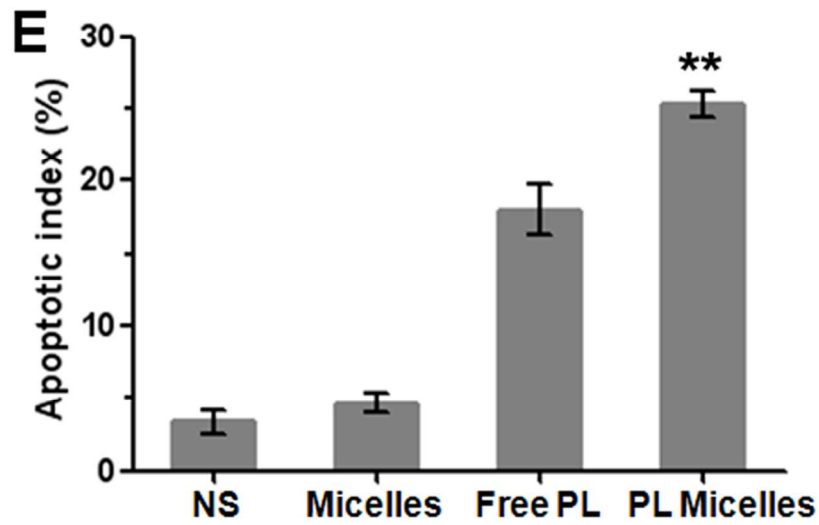
TUNEL immunofluorescent staining of tumors. Representative TUNEL immunofluorescent images of NS (A), blank micelles (B), free PL (C), and PL micelles (D) group, and mean apoptotic index in each group (E), **p < 0.01 vs. free PL.
101x143mm (300 x 300 DPI)

Ki-67 immunohistochemical staining of tumors. Representative Ki-67 immunohistochemical images of NS (A), blank micelles (B), free PL (C), and PL micelles (D) group, and mean Ki-67 LI in each group (E), **p < 0.01 vs. free PL.

127x182mm (300 x 300 DPI)
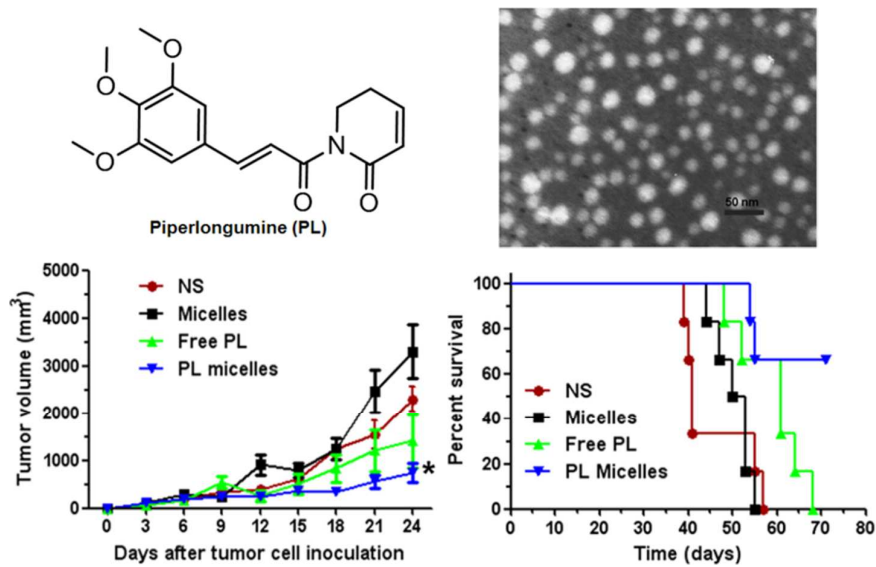
Piperlongumine was rendered into polymeric micelles to form nanoassemblies, which significantly suppressed tumor growth and prolonged survival of tumor-bearing mice.